Supplementary information

Recovery of crystalline silicon from waste solar cells by green deep eutectic solvent - hydrogen peroxide system

Ruying Yang,[a] Nengwu Zhu,[*a,b,c,d] Yunhao Xi,[a] Sunjuanzi Gao,[a] Pingxiao Wu,[a,b] Zhi Dang[a,b]

a. School of Environment and Energy, South China University of Technology, Guangzhou 510006, PR China

b. The Key Laboratory of Pollution Control and Ecosystem Restoration in Industry Clusters Ministry of Education, Guangzhou 510006, PR China

c. Guangdong Environmental Protection Key Laboratory of Solid Waste Treatment and Recycling, Guangzhou 510006, PR China

d. Guangdong Provincial Key Laboratory of Solid Wastes Pollution Control and Recycling, Guangzhou 510006, PR China

* E-mail: nwzhu@scut.edu.cn

Table of contents:

1. Characterization of synthesized DES (Text S1).
2. Apparent activation energy calculation (Text S2).
3. Technical data of the polycrystalline silicon solar panel (Table S1).
4. Kinetic fitting of Ag leaching in DES-H_2O_2 aqueous solution system and DES aqueous solution system (Table S2).
5. Arrhenius fitting of Ag leaching in DES-H_2O_2 aqueous solution system and DES aqueous solution system (Table S3).
6. Binding energies of the Ag complexes (Table S4).
7. Flow chat of pretreatment of photovoltaic panels and recovery of silicon wafers (Fig. S1).
8. Chemical reaction for DES synthesis by ChCl and OA (Fig. S2).
9. FT-IR (a) and 1 H NMR (b) spectra of OA, ChCl and DES, and TG-DSC of DES (c) (Fig. S3).
10. The leaching efficiency of silver in DES-H_2O_2 aqueous solution system (a) and DES aqueous solution system (b) (Fig. S4).
11. Arrhenius fitting of silver leaching in DES-H_2O_2 aqueous solution system (a) and DES aqueous solution system (b) (Fig. S5).
12. UV-vis spectra of DES, DES after experiment, Ag^+ in DES and Al^{3+} in DES (Fig. S6).
13. HRMS spectra after DES leaching: (a) negative mode and(b) positive mode (Fig. S7).
14. The preferred structures of silver complexes (Fig. S8).
15. Surface diagrams of silicon wafer after removing Si3N4 under different conditions (Fig. S9).
16. XPS spectrum of the front side of recycled silicon wafer (Fig. S10).
17. Photographs of front and back sides of silicon cell in different stages (Fig. S11).

Text S1

The synthesized DES involving hydrogen bonding interaction was characterized by FTIR and ^{1}H NMR (Fig. S3). The FTIR spectra of oxalic acid, choline chloride and DES in the range from 400-4000 cm^{-1} could be seen in Fig. S3a. The characteristic peaks in the synthesized DES were shown from the vibrations at 3327, 1723, 1478, 1185 and 950 cm^{-1}, of which all distinctive bands of the two components were contained. Specifically, the existences of N-C single bond (the most obvious signature of choline chloride) and quaternary ammonium ion in choline chloride were indicated by the peaks at 1478 and around 950 cm^{-1}, respectively. C=O and C-O vibrations in oxalic acid were associated with the vibrations at 1723 and 1185 cm^{-1}. The formation of hydrogen bonding was mainly judged by the movement of the O-H peaks. To more specific, the O-H vibrational region in oxalic acid contained a broad overlapping band centered at 3097 cm^{-1}, which was a strongly bonded dimer ring of carboxylic acids formed by intermolecular hydrogen bonding between C=O and O-H. Whereas, the peak of the O-H vibration was changed from 3097 cm^{-1} in oxalic acid and 3219 cm^{-1} in choline chloride to 3327 cm^{-1} after DES was produced, it was possible that the hydrogen bonding contact was largely formed between Cl^{-} of choline chloride and -OH of oxalic acid. The ^{1}H NMR spectrum could further verify the existence of hydrogen bonding interaction between choline chloride and oxalic acid. The proton of hydroxyl group in choline chloride shifted to a lower field (from 3.25 to 2.90 ppm), which referred to the presence of OH-Cl hydrogen bonding interaction. Overall, the choline chloride and oxalic acid-based DES was successfully synthesized with the formation of hydrogen bonding.

To clarify the temperature range for leaching, the thermal stability of DES was shown with TGA-DSC from 35 to 450 °C at N_2 atmosphere (Fig. S3c). A small weight loss of less than 2 %

occurred from 35 to 100 °C corresponding to the evaporation of small amounts of residual water. With the increase of temperature to about 140 °C, a sharply weight loss of 53 % was detected due to the decomposition of oxalic acid and small amounts of choline chloride. With a further increase of temperature, another massive weight loss was performed around 280 °C, which connected to the complete decomposition of choline chloride. Herein, the maximum work temperature of 140 °C was revealed from the two stages, at which the DES could maintain its liquid state for a steady operation. Since less molecules were activated at low temperature while hydrogen peroxide decomposed rapidly at high temperature, 80 °C was chosen as the leaching temperature.

Text S2

Apparent activation energy of the DES and DES-H_2O_2 system from kinetic experiments was used to explore the change in activation energy with or without H_2O_2. Since the reactants were solids and the products were soluble in solution, the leaching process was simulated using the shrinking core model, which was typically categorized as chemical reaction control (Eq. S1), diffusion control (Eq. S2) and chemical reaction- diffusion mixing control (Eq. S3).

$$1-(1-x)^{1/3}=k_1t \quad (S1)$$

$$1-2/3x-(1-x)^{2/3}=k_2t \quad (S2)$$

$$1/3\ln(1-x)+(1-x)^{-1/3}-1=k_3t \quad (S3)$$

where k_1, k_2 and k_3 refers to reaction rate constants for different control stages, t is reaction time (min) and x is silver leaching rate.

In order to compare the activation energy of silver leaching in the two system, we performed a kinetic analysis on the DES-H_2O_2 aqueous solution system and DES aqueous solution system. The silver leaching efficiency of silver in the two systems was shown in Fig. S4.

The kinetic analysis was performed with the silver leaching efficiency and Eqs. S1-S3. The fitting results were shown in the Table. S2. For DES-H_2O_2 aqueous solution system, the fit of the three control models was close but the intercept of the fitting line of mixing control was closer to zero, hence, the Ag leaching in DES-H_2O_2 aqueous solution system could be considered to be more compatible with the mixing control process. For DES aqueous solution system, the better fit was performed in chemical reaction control, which could consider the Ag leaching was controlled by chemical reaction process.

In order to obtain the apparent activation energy of the silver leaching process in the two systems, the reaction rate (k) and temperature (T) were fitted using the Arrhenius model (Eq. S4) with the variation formula of Eq. S5. The Arrhenius fitting curve and the data of the two systems were shown in Fig. S5 and Table. S3, respectively.

$$k=Ae^{-Ea/RT} \quad (S4)$$

$$\ln k=\ln A+\frac{-Ea}{RT} \quad (S5)$$

where k refers to reaction rate constant, A refers to indexing factor, Ea is apparent activation energy (kJ/mol), R is molecular gas constant (8.314 J/(K·mol)), and T is thermodynamic temperature (K).

Based on the fitting process, the apparent activation energy of silver leaching in DES-H_2O_2 and DES system were calculated as 24.133 and 123.521 kJ/mol, respectively. Hence, the activation energy of silver leaching decreased with adding H_2O_2 was concluded.

Table S1 Technical data of the polycrystalline silicon solar panel.

Item	Description
Type	Polycrystalline Silicon
STC Power Rating	330 W
Length×Width×Depth	2000×992×40 mm
Weight	26 kg
Number of Cells	72 (156×156 mm)

Table S2 Kinetic fitting of Ag leaching in DES-H_2O_2 aqueous solution system and DES aqueous solution system.

system	temperature /K	chemical reaction	R^2	diffusion	R^2	mixed	R^2
DES-H_2O_2	323	k_1t=0.0027x +0.0686	0.9211	k_2t=0.0007x -9E-05	0.9559	k_3t=0.0007x -0.0033	0.9680
	338	k_1t=0.0036x +0.0682	0.9639	k_2t=0.0011x -0.0036	0.9867	k_3t=0.0011x -0.0097	0.9862
	353	k_1t=0.0027x +0.1654	0.9391	k_2t=0.0011x +0.0195	0.9239	k_3t=0.0015x +0.0034	0.8877
DES	323	k_1t=1E-05x-0.0002	0.9800	k_2t=1E-08x-2E-07	0.8615	k_3t=5E-09x-1E-07	0.8614
	338	k_1t=7E-05x-0.0007	0.8863	k_2t=3E-07x-7E-06	0.7588	k_3t=2E-07x-4E-06	0.7581
	353	k_1t=0.0005x -0.0049	0.9923	k_2t=1E-05x-0.0002	0.912	k_3t=6E-06x-0.0001	0.9077

Table S3 Arrhenius fitting of Ag leaching in DES-H_2O_2 aqueous solution system and DES aqueous solution system.

System	Arrhenius fitting	R^2	Ea (kJ/mol)
DES-H_2O_2	lnk=-2902.7/T+1.7394	0.9934	24.133
DES	lnk=-14857/T+34.454	0.9992	123.521

Table S4 Binding energies of the Ag complexes.

Complex	E/(kJ/mol)	ΔE/(kJ/mol)
$[AgCl_2]^-_{uncomplex}$	-492.89	-629.89
$[AgCl_2]^-_{complex}$	-1122.78	
$[Ag(OH)Cl]^-_{uncomplex}$	-1385.90	-365.89
$[Ag(OH)Cl]^-_{complex}$	-1751.79	
$[AgHC_2O_4Cl]^-_{uncomplex}$	-5338.52	-224.74
$[AgHC_2O_4Cl]^-_{complex}$	-5563.26	
$[Ag_2(HC_2O_4)_2Cl_2]^{2-}_{uncomplex}$	-10677.04	-401.50
$[Ag_2(HC_2O_4)_2Cl_2]^{2-}_{complex}$	-11078.54	

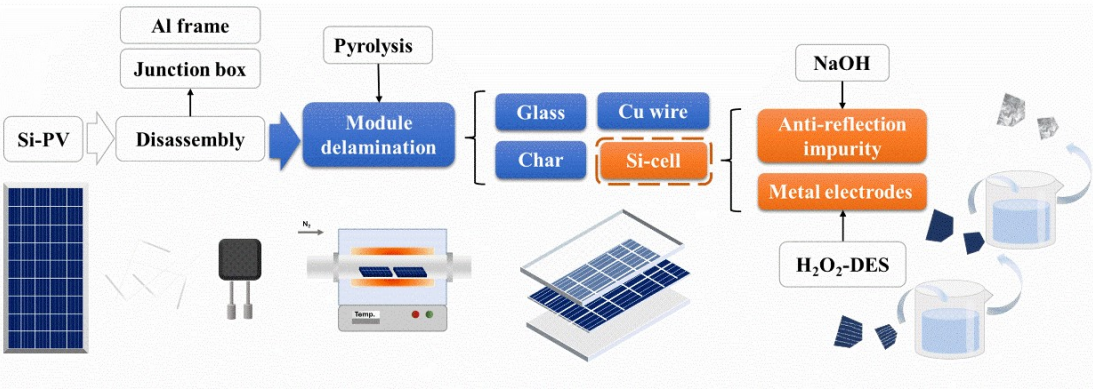

Fig. S1 Flow chat of pretreatment of photovoltaic panels and recovery of silicon wafers.

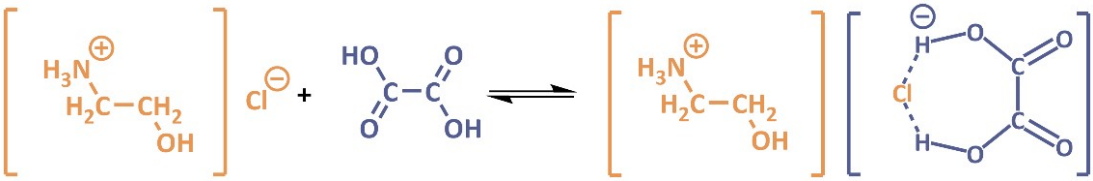

Fig. S2 Chemical reaction for DES synthesis by ChCl and OA.

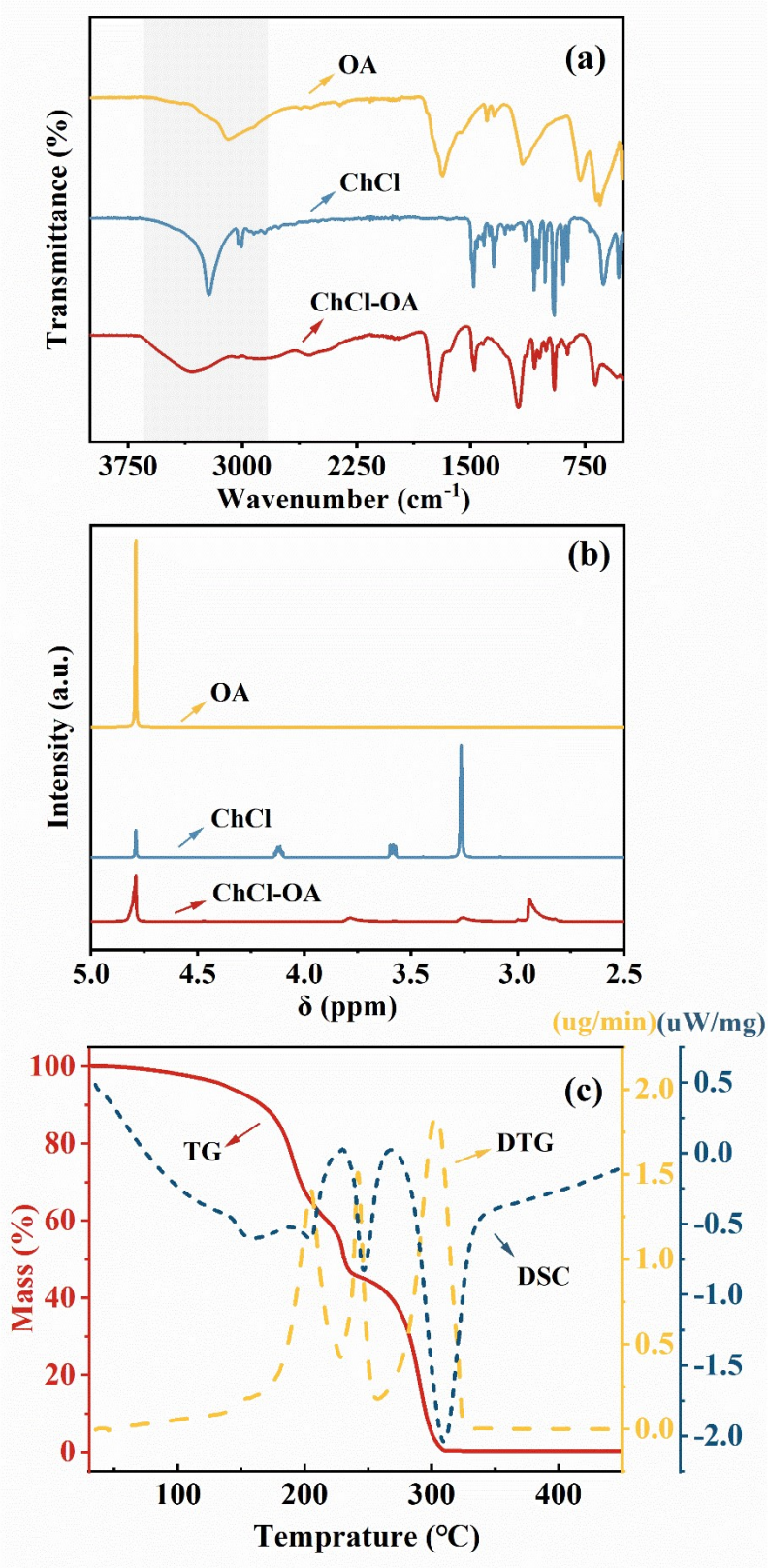

Fig. S3 FT-IR (a) and ^{1}H NMR (b) spectra of OA, ChCl and DES, and TG-DSC of DES (c).

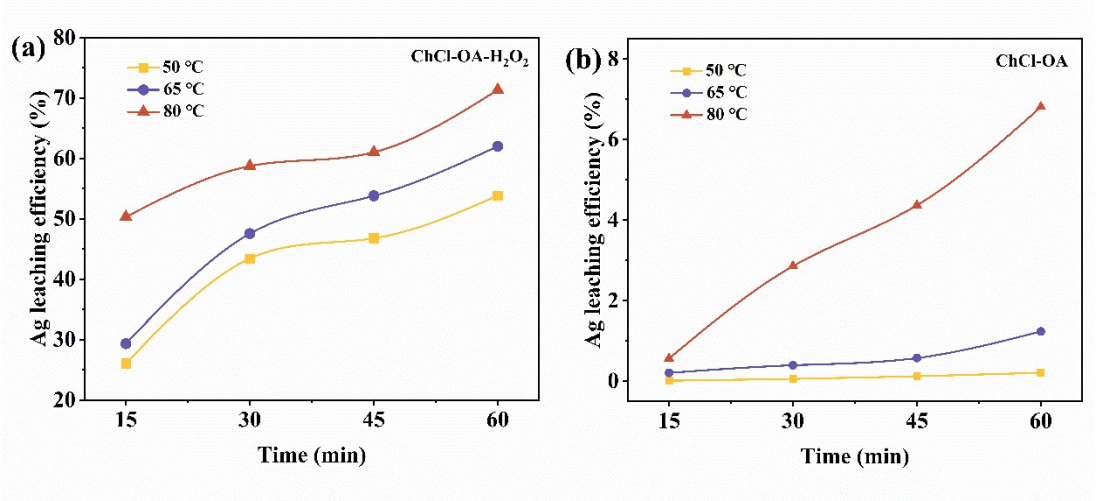

Fig. S4 The leaching efficiency of silver in DES-H_2O_2 aqueous solution system (a) and DES aqueous solution system (b).

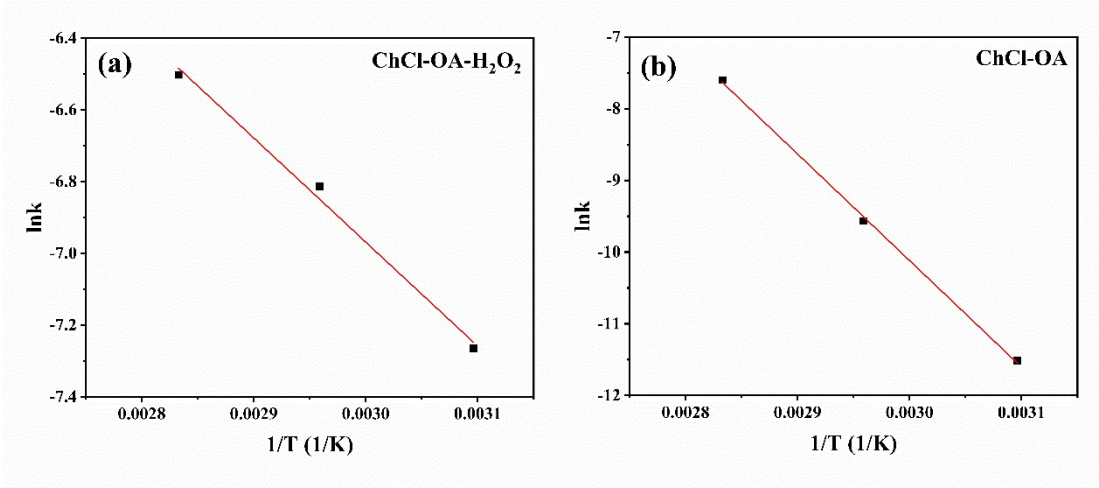

Fig. S5 Arrhenius fitting of silver leaching in DES-H_2O_2 aqueous solution system (a) and DES aqueous solution system (b).

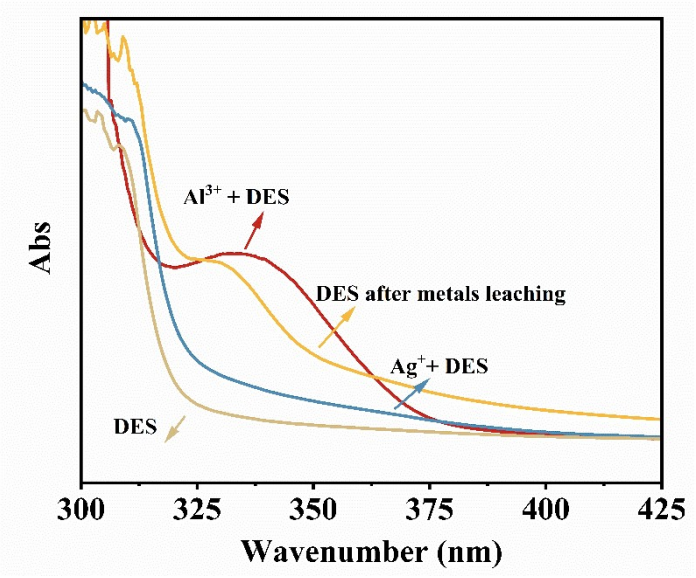

Fig. S6 UV-vis spectra of DES, DES after experiment, Ag^{+} in DES and Al^{3+} in DES.

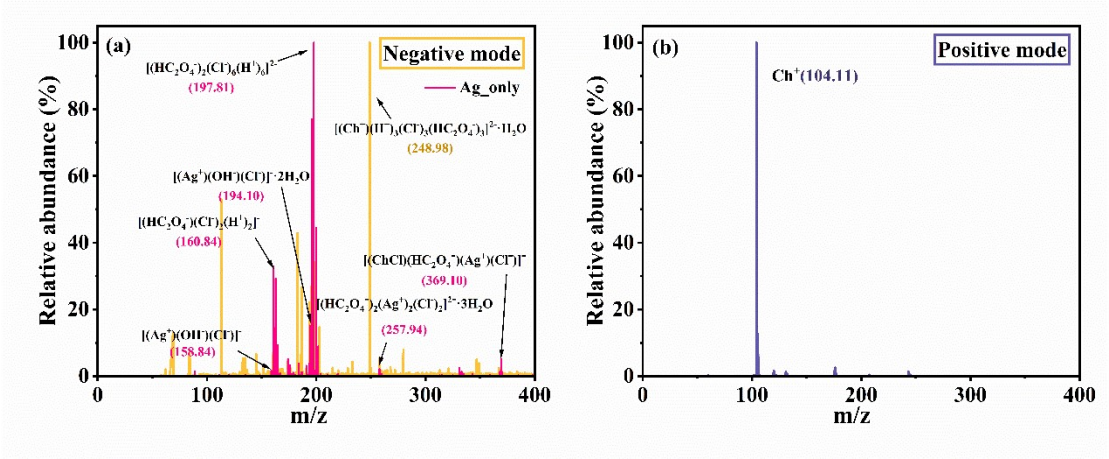

Fig. S7 HRMS spectra after DES leaching: (a) negative mode and(b) positive mode.

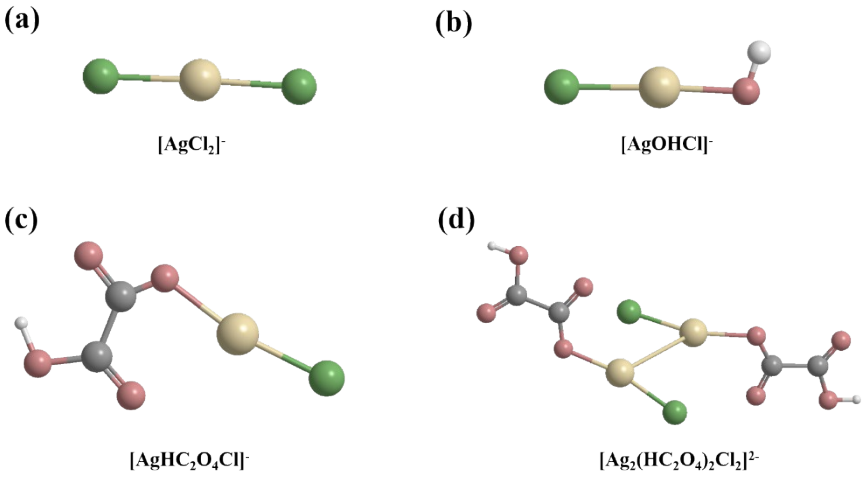

Fig. S8 The preferred structures of silver complexes.

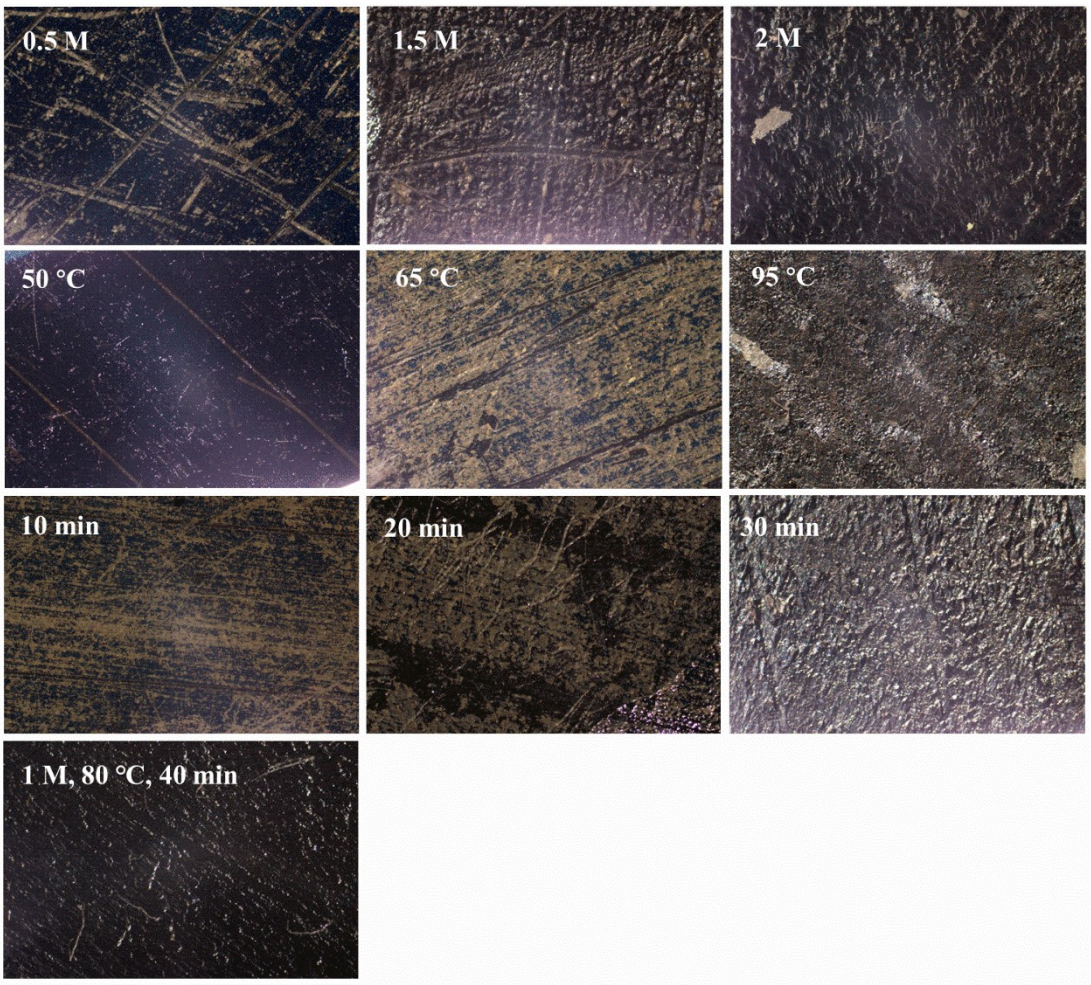

Fig. S9 Surface diagrams of silicon wafer after removing Si_3N_4 under different conditions.

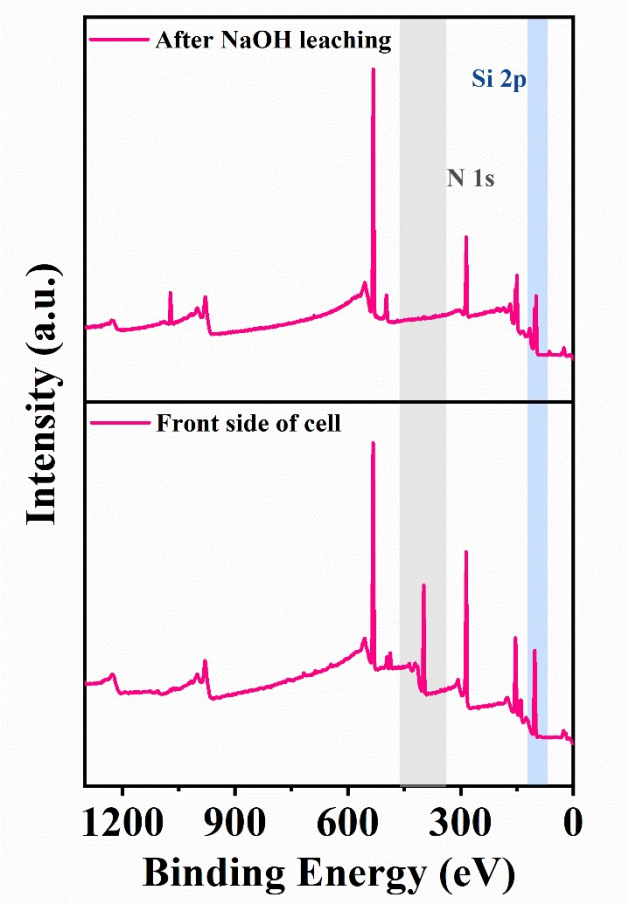

Fig. S10 XPS spectrum of the front side of recycled silicon wafer.

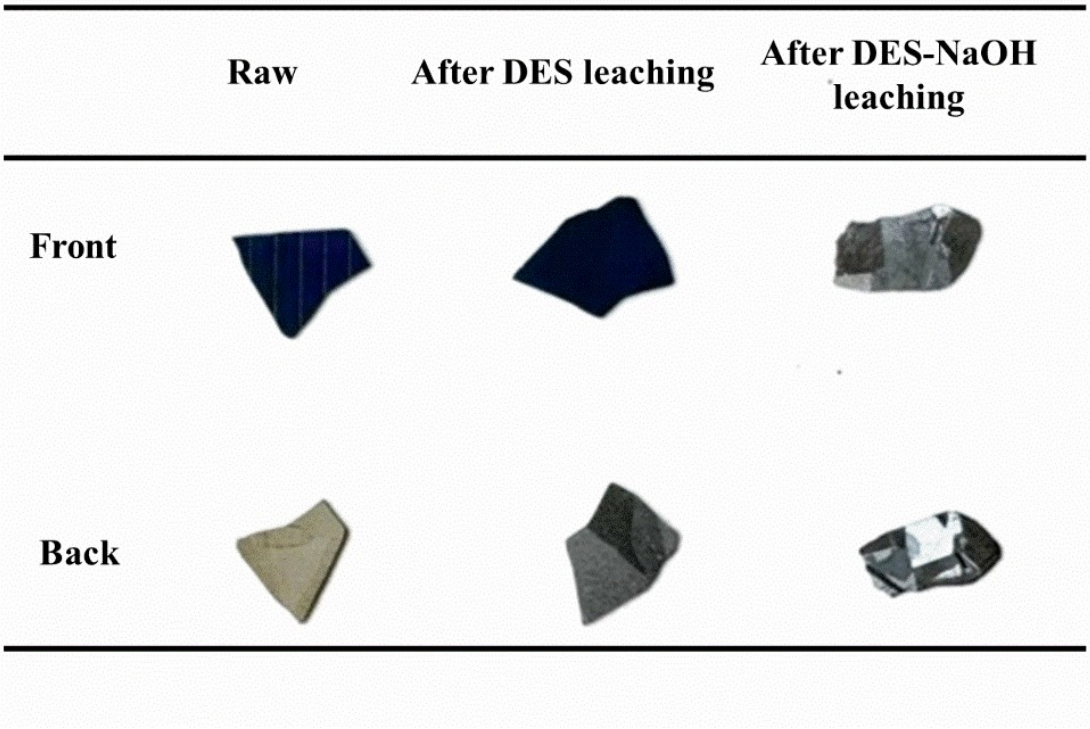

Fig. S11 Photographs of front and back sides of silicon cell in different stages.